A New *In Vitro* Model to Evaluate Differential Responses of Endothelial Cells to Simulated Arterial Shear Stress Waveforms

Brett R. Blackman

Guillermo García-Cardeña

Michael A. Gimbrone, Jr.[1]

Center for Excellence in Vascular Biology,
and Department of Pathology,
Brigham and Women's Hospital
and Harvard Medical School,
Boston, MA 02115

In the circulation, flow-responsive endothelial cells (ECs) lining the lumen of blood vessels are continuously exposed to complex hemodynamic forces. To increase our understanding of EC response to these dynamic shearing forces, a novel in vitro flow model was developed to simulate pulsatile shear stress waveforms encountered by the endothelium in the arterial circulation. A modified waveform modeled after flow patterns in the human abdominal aorta was used to evaluate the biological responsiveness of human umbilical vein ECs to this new type of stimulus. Arterial pulsatile flow for 24 hours was compared to an equivalent time-average steady laminar shear stress, using no flow (static) culture conditions as a baseline. While both flow stimuli induced comparable changes in cell shape and alignment, distinct patterns of responses were observed in the distribution of actin stress fibers and vinculin-associated adhesion complexes, intrinsic migratory characteristics, and the expression of eNOS mRNA and protein. These results thus reveal a unique responsiveness of ECs to an arterial waveform and begin to elucidate the complex sensing capabilities of the endothelium to the dynamic characteristics of flows throughout the human vascular tree. [DOI: 10.1115/1.1486468]

Keywords: Blood Flow, Mechanotransduction, Migration, eNOS

Introduction

In the human circulatory system, blood flow in arteries is highly dynamic and variable. For a typical waveform, the contraction of the heart during systole forces blood to accelerate through the arteries within 100–200 milliseconds. As the heart expands to collect blood during diastole, arterial flow will decelerate in 200–300 milliseconds, briefly reverse in direction, and then reverse again and continue distally to a low forward basal flow until the next cycle. The velocity characteristics of an arterial waveform (e.g., peak amplitude, flow reversal, pulsation frequency) are variable throughout the vasculature and are dependent on local geometry, elasticity of the artery wall, peripheral vascular resistance, and heart rate [1]. As a result of these dynamic flow patterns, a complex set of mechanical forces (e.g., shear stress, hydrostatic pressure, and hoop stress) are continuously imposed on the endothelial lining of these vessels. Endothelial cells (ECs) have been shown to be highly responsive to these biomechanical forces [2], and recent studies have provided insights into several mechanisms involved in mechanotransduction [2–5].

Over the past twenty years, various models have been designed to simulate the effects of the blood flow environment on cultured ECs in an effort to understand their response to biomechanical forces. These devices are designed to generate either a single type of stimulus (e.g., shear stress, hydrostatic pressure, hoop stress) or a combination of stimuli [2]. Models investigating the influence of shear stress alone on EC response have simulated steady laminar [6], sinusoidal (net forward with and without reversing) and oscillatory [7–9], disturbed (i.e., spatial-varying) [10], and turbulent (i.e., random temporal and spatial varying) flows [11–13]. Results from these studies demonstrate the ability of the EC not only to sense shear stress stimuli, but also to discriminate among distinct types of flow patterns. It is becoming more apparent that the exact nature of the flow stimulus *in vitro* regulates EC phenotype [14] and is hypothesized that the local hemodynamic environment *in vivo* can contribute to regional differences in EC phenotype [15].

Recently, several models have attempted to simulate an arterial-like flow environment by imposing aortic pressure waves or controlled flow rates onto an endothelialized tubular model [16–18]. These models inherently contain a combination of stimuli that are interdependent (e.g., flow, pressure, strain), which influences the input or response of another stimuli. Although this model incorporates similar flow characteristics encountered by an intact vessel, which may be important in endothelial response, a shear stress flow model provides a more exact relationship between a well defined biomechanical force and a measurable biological response without the influence of a deformable substrate. Langille [19] was the first to demonstrate in a parallel rotating disk model (i.e., shear stress only) the application of an arterial-like waveform on the endothelium of dog aortic tissue. This model, which exposed the tissue to a linear spatial gradient in shear stress, investigated the influence of high levels of shear stress (up to 2000 dyn/cm^2) on endothelial injury, adhesion strength, and thrombogenic response. More recent models demonstrate the ability to deliver complex pulsatile flows [20,21], though a systematic study evaluating the effects of arterial-like shear stress patterns on EC response has yet to be conducted.

In an effort to better approximate the actual wall shear stresses experienced by ECs in arterial geometries *in vivo*, and to understand how these stimuli affect endothelial phenotype, we have undertaken the design and development of a novel cone-plate flow system to deliver pulsatile shear stresses in an arterial-like waveform that mimics similar characteristics of flow in different human arteries. The responsiveness of ECs to an arterial-like shear stress stimulus is evaluated in terms of cell morphology, migratory be-

havior, adaptation of cytoskeletal-associated proteins, and the regulation of endothelial nitric oxide synthase (eNOS) mRNA and protein expression.

Methods

The Dynamic Flow System (DFS). The dynamic flow system (DFS) is a multi-component cone and plate device that comprises a culture well environment and main drive unit (cone assembly and motor). The design of this system is a modification of a previously described model [21]. The complete system mounts onto a microscope stage and, with a transparent cone (0.5° cone angle) and plate surface (10.8 cm-diameter), the cells are visualized under dynamic flow conditions via phase microscopy (Fig. 1a). Real-time changes may also be monitor using fluorescence video microscopy to detect fluorescently tagged proteins or indicators (e.g., to monitor intracellular pH or calcium).

Velocity waveforms generated by the drive system are controlled with microstepper motor technology (Parker Hannifin, Rohnert Park, CA). Through software (Compumotor 6000, Rohnert Park, CA), the fluid dynamics can be programmed to simulate waveforms ranging from uniform laminar flows to more complex arterial waveforms. Precise control of the motor permits real-time, or "on-the-fly" changes in acceleration/deceleration rates and flow directions, which are important features for replicating arterial-type flows. The precision at which the programmed waveforms are replicated by the motor is ~0.02% (reported by the manufacturer). As documented in a previous report, the inertial effects for the startup problem (i.e., a ramp and hold flow condition) in a cone and plate geometry were negligible with minimal lag time at the greatest radii and acceleration times on the order of 10 milliseconds, thus demonstrating that the shear stress on the plate surface maps, in a temporal manner, that of the cone's velocity [21].

The device also includes several features critical for maintaining a physiological environment. Two access ports in the well permit constant exchange of fresh media. These ports can be used to introduce pharmacological agents without disturbing the experiment or flow environment. An external heater (Atlantic Thermal Co., Hopedale, MA) is configured to control the culture temperature at 37°C, and a plastic enclosure over the apparatus maintains the internal environment at 5% CO_2 in humidified air. Experiments validating the DFS demonstrated that the materials used to fabricate and sterilize the well environment were non-toxic to an endothelial cell monolayer up to 5 days in culture.

Development of Arterial Shear Stress Waveform. Blood flow patterns in large arteries (e.g., thoracic, abdominal, carotid, brachial arteries) share similar time-varying characteristics throughout a cardiac cycle. To develop an arterial-like shear stress waveform that would incorporate similar characteristics, we selected as a model a previously defined waveform captured from the abdominal aorta of a normal human subject using phase-encoding magnetic resonance imaging technique [22]. This waveform encompass several common temporal features found in large arteries (e.g., acceleration/deceleration rates, flow reversal, forward basal flow).

To translate this waveform from mean (centerline) velocity measurements in the aorta to shear stress values at the vessel wall, the equation of *circular* Poiseuille flow was used to approximate shear stress. It is important to note that the Womersley Number for this vessel is approximately 10.6 (based on a mean lumen diameter of 17 mm, a blood viscosity of 4 cP, and frequency of 1 Hz), indicating there is a significant influence of the transient inertial forces in this region of the aorta. Therefore, theoretically, Poiseuille's Law would underestimate the shear stress values. However, the computed maximum and minimum shear stress for this waveform using Poiseuille's Law (~30 dyn/cm² and −7.5 dyn/cm², respectively) coincided with the range of near wall shear stress measurements made in vivo [23,24]. Initial flow
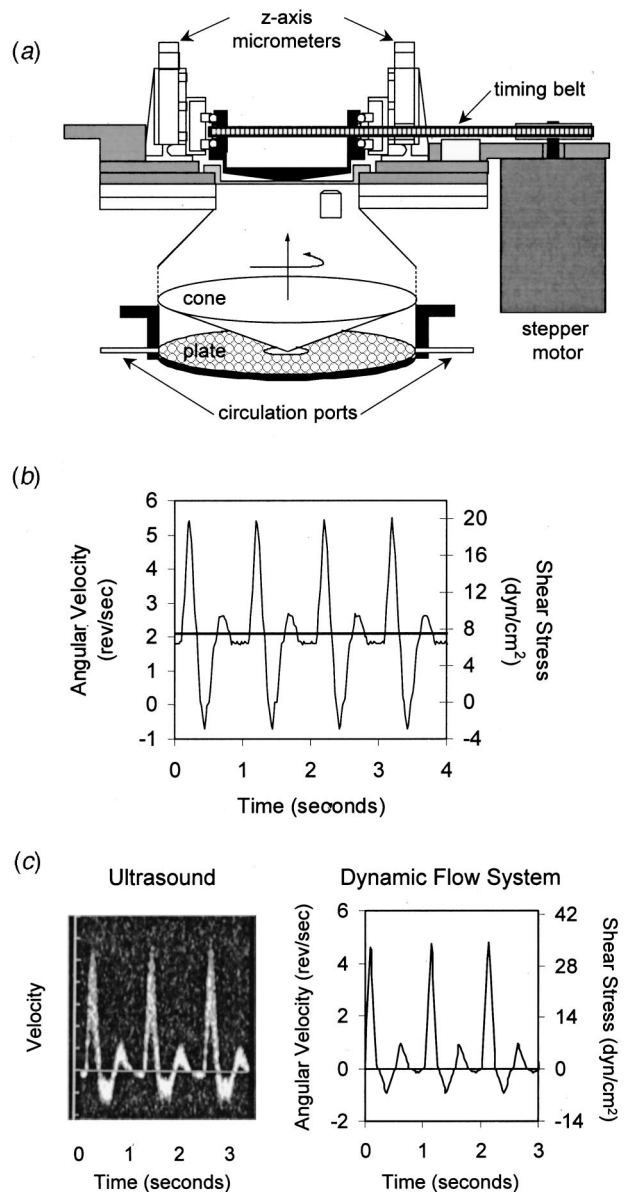

Fig. 1 Schematic of the Dynamic Flow System and plot of motor-generated arterial waveforms. (*a*) The DFS is a cone and plate device that mounts on to a microscope stage and permits direct visualization of the cells adhered to the plate surface. The rotation of the cone is controlled via a timing belt connection to the programmable stepper motor. (*b*) An arterial waveform, developed from phase-encoding MRI of a previously characterized human abdominal aorta [22], was programmed into DFS and used to assess the biological response of ECs for all experiments in this study. Measurements from the DFS are represented for multiple cardiac cycles. Characteristics of this waveform include, a peak shear stress of 20 dyn/cm² during systole, flow reversal during diastole to a maximum of −3 dyn/cm², an equivalent time-average of 7.5 dyn/cm² (depicted by the solid horizontal line), and a pulsation frequency of 1Hz. (*c*) A blood flow waveform acquired by ultrasound from the brachial artery of a normal human subject (left panel) was programmed into and measured from the DFS (right panel). Plots represent multiple cardiac cycles of the waveform, and the programmed waveform is modeled at a frequency of 1Hz. For the measured waveforms, (*b*) and (*c*, right), values of the angular velocity (rev/sec) were measured directly from the motor, and values of shear stress (dyn/cm²) were computed at the plate surface.

experiments in this model demonstrated that high shear stress rates (SSR) (>300 dyn/cm^2/sec) compromised the integrity of the monolayer at the end of 24 hour pulsatile flow experiments. As a result, the shear stress values of this waveform was modified by decreasing the maximum shear stress during systole to 20 dyn/cm^2 (SSR~ 200 dyn/cm^2/sec) and increasing the shear stress during the diastolic phase in order to maintain a physiological level of time average shear stress (7.5 dyn/cm^2) [23,24]. In defining the time history of the shear stress waveform relative to the blood flow velocity pattern, Ling et al. [25] previously had demonstrated that temporal patterns in blood flow in the thoracic aorta of a dog approximate the time-varying shear stress patterns as computed from the full Navier-Stokes equations. Other factors, which would influence the actual wall stress magnitude and temporal histories, such as vessel wall compliance, were taken into account in the latter computation [26]. Therefore, the temporal characteristics of the waveform used in this report were reproduced from the blood flow patterns of the model waveform. The values of shear stress were converted to angular velocity using the following equation for a cone and plate viscometer, $\tau = \mu \omega / \alpha$, where $\tau =$ shear stress, $\mu =$ dynamic viscosity, $\omega =$ angular velocity, and $\alpha =$ cone angle (0.5°, 0.00873 radians). The waveform was segmented into discrete time steps and programmed via a point to point method into the DFS. To validate this waveform directly from the apparatus, an encoder (Danaher Controls, Gurnee, IL) and digital acquisition unit (US Digital Corp., Vancouver, WA) were used to acquire speed versus time data.

Validation of Fluid Mechanics. To validate the fluid dynamics of the DFS under steady and time-varying aspects of the arterial flow, 10 μm fluorescent (FITC) latex microspheres (1:125 in water; Polysciences, Inc., Warrington, PA) were used as a marker for tracking the dynamic motions of the fluid. Image sequences were acquired at video frame rate (1/30 sec) using a high-speed video recorder (Sony) and a fluorescence microscope (Nikon TE300, Nikon) with an FITC filter.

Cell Culture and Experimental Protocol. Human umbilical vein ECs (HUVEC) isolated from normal term cords and pooled from multiple (5 to 7) donors were cultured in complete media (Medium 199 with 25mM HEPES (Biowhittaker), 20% fetal calf serum (Gibco) and supplemented with 2mM L-glutamine (Gibco), 50 μg/ml endothelial cell growth supplement (Biomedical Technologies), 100 μg/ml heparin (Sigma), and 100 unit/ml penicillin-G+100 μg/ml streptomycin (Biowhittaker)) and incubated at 37°C in 5% CO$_2$ in humidified air.

For the flow experiments, high molecular weight dextran (Mw. ~ 460 kD; Sigma) was used to increase media viscosity, which was measured prior to each experiment using cone-plate viscometer (Brookfield Engineering Laboratories, Inc., Stoughton, MA). This value was used to calculate the corresponding angular velocity in order to achieve a consistent shear stress output. The mean viscosity for all experiments was 2.11 ± 0.05 cP (n=30).

For each experimental set, HUVEC were plated from the same pooled batch (subculture 1) at an initial density of 70,000 cells/cm^2 onto a 0.1% gelatin (Sigma) coated 100 mm culture dish for static controls and a custom designed 10.8 cm diameter polystyrene plate surface (Plaskolite, Inc., Columbus, OH) for flow experiments. To eliminate potential shear-induced wounding of the endothelium at the center of the plate, a silicone rubber plug (class VI medial-grade, 3.18 cm diameter) was used to void the center of any cell adhesion or growth. The plug was removed just prior to the start of an experiment. Confluent monolayers were maintained for 48 hours in complete medium and stored at 37°C in 5% CO$_2$ in air.

At the start of the experiment, static control cells and cells in the cultured well apparatus were rinsed once with warm (37°C) Dulbecco's phosphate buffer saline (DPBS) then submerged in complete media containing 2% (w/v) dextran. The well was placed into a custom base mounted on the microscope stage, and

the cone was manually lowered into position. The cells were then exposed to a steady laminar shear stress (LSS) of 7.5 dyn/cm^2 or an arterial pulsatile flow (ART) with an equivalent time-average shear stress of 7.5 dyn/cm^2 and a frequency of 1Hz for 24 hours (Fig. 1b). At the start of each experiment, flow was automatically ramped up using a linear profile to a "steady" waveform in 5 minutes. For ART flow, the amplitude of the arterial function increased linearly with time over the initial 5 minutes (not shown). Fresh complete media containing 2% dextran was exchanged through the side ports at a volume flow rate of 0.07 ml/min, which corresponded to one complete exchange of the medium each hour.

Immunofluorescence and Confocal Imaging. To prepare cells for immunofluorescence staining, cultures were immediately rinsed twice in warm (37°C) PHEM buffer (60mM PIPES, 25mM HEPES, 10mM EGTA, 2mM MgCl$_2$, and pH 6.9). For plectin, cells were fixed in 4% paraformaldehyde in DPBS for 10 minutes at 37°C and permeablized in 0.2% Triton X-100 for 5 minutes at room temperature. For vinculin, cells were initially permeabilized for 2 minutes with a modified PHEM buffer (PHEM pH 6.9, $2\mu M$ phallacidin (Sigma), $20\mu M$ taxol (Sigma), 1mM GTP (Sigma), 0.75% TritonX-100) and fixed in 4% paraformaldehyde in DPBS containing 5mM MgCl$_2$ and 10mM EGTA for 10-minutes. Cells were then rinsed in 0.1% bovine serum albumin (BSA) in DPBS and incubated in 1% BSA for 40 minutes to block non-specific binding. Monolayers were incubated with antivinculin antibody (1:100, mouse monoclonal V9131, Sigma) or antiplectin antibody (1:500, guinea pig polyclonal, Research Diagnostics Inc.) for 1hr at room temperature, rinsed well with 0.1% BSA in DPBS, and blocked for 30 minutes with 2% goat serum in DPBS. Secondary antibodies, goat anti-mouse (1:200, Alexa Fluor 546, Molecular Probes) for vincluin and goat anti-guinea pig (1:200, Alexa Fluor 488, Molecular Probes) for plectin, were incubated for an additional 1 hr at room temperature, rinsed in DPBS, and mounted using Gel-Mount (Biomedia).

For visualizing actin, fixed and permeablized cells were incubated with Oregon green 514 phalloidin (1:20, Molecular Probes) for 1 hr at room temperature, rinsed three times in DPBS, incubated with sytox orange (0.01%, Molecular Probes) for 2 minutes to stain nuclei, and mounted in Gel-Mount.

A Leica TCSNT confocal laser-scanning microscope was used to acquire serial sections of images as previously described [14]. Briefly, images were taken sequentially in the z-axis from the apical to basal surface at 0.2 μm increments and a 0.2 μm pixel size resolution with a 40× oil immersion lens and a 1.5 times digital zoom. For actin and plectin, sytox stained nuclei were used as fiduciary markers to identify the center of the nucleus. The image corresponding to the nuclei with the highest intensity was chosen as the centerline, or reference image. To evaluate the apical structures of these proteins, five sequential images starting with centerline image and moving toward the apical surface were merged to represent a 1 μm thick apical section. For vinculin, a single image was acquired at the basal surface of the monolayer.

Image Analysis. Time-lapse images of the endothelium were acquired (Image Pro Plus, Media Cybernetics, Rockville, MD) at 2 minute intervals for static and 24 hr flow experiments using a 4×objective and phase optics. A custom macro was applied to the movie sequence to: 1) sub-sequence the movie into 6 minute time intervals, 2) apply a series of routines to optimize cell border contrast, and 3) skeletonize the resulting sequence using a pruning feature that traces the boundaries of each cell. As a result, each image was transformed into tracings of the cell borders. These images were then superimposed onto the sub-sequenced phase images to confirm accurate tracings of the cell perimeters. For each image, Image Pro Plus assigned an object number to each cell. Using the image analysis software, x-y centroid of each cell (object) and the mean aspect ratio in the imaging field was measured and exported to an Excel spreadsheet for further analysis.

To evaluate cell migration, a custom program was developed in

MatLab (MathWorks, Natick, MA) to trace the paths of single cells over the 24 hour time period from the resultant x-y data. This was necessary since object numbers were reassigned among successive images. The program then evaluated the coordinates for subsequent time intervals using a minimum distance traveled algorithm. The resultant cell path matrix yielded x-y coordinates as a function of time, which was converted from pixels to spatial distances in micrometers. A sub-program read in the cell path matrix and evaluated two intrinsic migratory characteristics, the root mean square (RMS) cell speed, S, and directional persistence, P. Computation of these two values was based on the equation derived for the mean square displacements, $\langle D^2 \rangle$, as describe by Dunn [27],

$$\langle D^2 \rangle = S^2 P^2 (T/P - 1 + e^{-T/P})$$

where, T equals the time intervals that $\langle D^2 \rangle$ was calculated over. A non-linear least squares curve-fit routine was used to solve for these two coefficients. These values were evaluated for individual cells and are representative of the migratory behavior for the entire 24 hours of the experiment.

Protein Isolation for Immunoblotting. Cells were immediately rinsed twice in cold (4°C) DPBS at the termination of the experiment. Protein was extracted in cold (4°C) lysis buffer (50mM Tris pH 7.5, 1% TritonX-100, 0.1% deoxycholate (Sigma), 50mM NaCl, 20mM leupeptin, 40uM aprotinin, 10ug/ml PMSF), scraped, collected, and sonicated on ice. Samples were rotated at 4°C for 1 hour prior to and following sonication, and then centrifuged at 14,000 rpm for 20 minutes at 4°C. The supernatant was collected and the protein concentration was evaluated using the Bio-Rad D_C protein assay (Bio-Rad, Hercules, CA). For each sample, $50\mu g$ of protein was added to $3\times$ denaturing sample buffer (0.5M Tris-HCl pH 6.8, 9% SDS, 9mM EDTA, 3.6% β-mercaptoethanol), boiled for 5 min, and then loaded and resolved in a 7.5% polyacrylamide gel. Protein was subsequently transferred from the gel onto a nitrocellulose membrane, blocked for 2 hours in 5% milk in Tris-buffered saline (TBS), incubated with anti-eNOS monoclonal antibody (Clone H32) in 5% milk in TBS for 2 hours, rinsed thoroughly in TBS, incubated with horseradish peroxidase-conjugated goat-anti-mouse (1:10,000, Jackson Laboratories), and rinsed again in TBS. Protein bands were visualized using ECL chemiluminescence (Amersham Pharmacia Biotech) and developed with Biomax film (Kodak). The intensity of each protein band per condition were assessed by densitometry and normalized to time-matched static controls.

Gene Expression Analysis. After exposure to the appropriate stimulus, cells were rinsed twice with ice-cold DPBS and scraped in Trizol (Gibco). RNA was isolated by ethanol precipitation and further purified and DNase-treated. RNA was transcribe using a MultiScribe based RT reaction. The following primers and Taqman probe were used: forward primer, 5'-CGGCATCACCAGGAAGAAGAC-3'; reverse primer, 5'-TCACTCGCTTCGCCATCAC-3'; and Taqman probe 5'-TGGCCAACGCCGTGAAGATCTCC-3', reactions were performed in a GeneAmp 5700 sequence detection system (Applied Biosystems).

Statistics. Statistical differences among experimental groups were evaluated either using a one-way ANOVA for post-hoc comparisons or the Student's t-test at a 95% confidence level and assuming equal variances.

RESULTS

Generation of Arterial Waveforms and Validation of the Fluid Mechanics. The goal of this study was to develop an *in vitro* flow model to simulate shear stress patterns similar to those experienced by the endothelium in different regions of the vasculature and evaluate the effects of this complex stimulus on EC response. An arterial-like waveform was selected from a previously defined waveform of the human abdominal aorta of a healthy volunteer that was well characterized by both magnetic resonance and ultrasound imaging techniques [22]. A modified version of this waveform was translated into a shear stress waveform and programmed into the DFS. Figure 1b shows this velocity trace measured directly from the stepper motor and depicts multiple cardiac cycles of the waveform. Values of angular velocity (rev/sec) were converted into units of shear stress (dyn/cm²) at the plate surface. The waveform includes several major characteristics, including a maximum shear stress of 20 dyn/cm² during peak systole, flow reversal during diastole that reaches -3 dyn/cm², a time-average shear stress of 7.5 dyn/cm², a frequency of 1Hz, and an oscillatory shear index [28] of 0.098. The biomechanical limits of this waveform (i.e., maximum, minimum, and time-average amplitude of shear stress) agree well with published results of near wall shear stress computations in the suprarenal and infrarenal region of the abdominal aorta using MRI techniques, in which maximum shear stress during systole ranged between 30 to 60 dyn/cm², minimum shear stress during flow reversal was -4 to -13 dyn/cm², and mean (time-averaged) shear stress ranged between 3 to 7 dyn/cm² [29,23,24]. The waveform in Figure 1b is used for all the arterial flow experiments in this study.

To further demonstrate the utility of the DFS to emulate complex flow patterns in different regions of the vasculature, blood flow measurements in the brachial artery of a normal human subject were acquired by ultrasound (Powervision 8000 Toshiba; Fig. 1c, left). In comparison to Figure 1b, the complexity of this waveform shares many characteristics with the waveform from the abdominal aorta. The flow pattern was translated into a shear stress waveform, as described in the methods, and programmed into the DFS. Figure 1c (right) shows the velocity trace acquired directly from the stepper motor and depicts multiple cardiac cycles at a frequency of 1Hz. The characteristics of this measured waveform were similar to those measured from ultrasound. Waveforms acquired from other vascular regions (e.g., human coronary and carotid artery) have been successfully modeled and programmed into the DFS (data not shown).

To validate the fluid mechanics of this system and demonstrate the dominance of viscous forces under steady and arterial flow, 10 μm fluorescent microspheres were visually tracked in the media through time. At steady state, laminar streaklines were observed throughout the fluid at constant speeds. This observation is consistent with the computed modified Re≪1, calculated at the maximum radius, indicating the flow is within the laminar regime and that secondary flows, computed from laminar flow theory, can be neglected, as previously described [30,31,21]. For the arterial waveform (Fig. 1b), the microspheres were observed to track the complex flow characteristics with no apparent effects of inertia (data not shown).

To evaluate the temporal and geometric limits in which shear stress tracks the input waveform for unsteady flow conditions, Stokes first and second problem were solved. Stokes first problem defines the diffusive time for the momentum of the fluid to reach a perpendicular distance of ~0.05 cm (the maximum height between the cone and the plate at max radius, 0.5° cone angle, 10.8 cm diameter surface) for an impulsively starting plate to be ~30 milliseconds. However, the value of the lag time is less for a defined acceleration as demonstrated in CFD solution by Blackman et al. [21] for a ramp and hold function. Therefore, in this system the tracking of shear stress at the plate surface, which scales with the radial distance, can be neglected for acceleration and deceleration features of the waveform greater than an acceleration or deceleration time of 20 milliseconds. For steady state conditions of a pulsatile function, Stokes second problem indicates that the diffusive distance (d) from the cone is constant, and for the parameters of the DFS is ~0.566 cm ($d = 4\sqrt{\nu/\omega_f}$; kinematic viscosity (ν) of 0.02 cm²/sec and a frequency (ω_f) of 1 Hz). Since this solution is based on a sinusoidal function, a Fourier

Series analysis was performed on the experimental waveform (Fig. 1b). This revealed that the waveform can be completely described within the first 10 harmonics ($\sim$90% of the magnitude up to the fifth harmonic). At the highest frequency component of this flow pattern, which is equivalent to the tenth harmonic, or 10 Hz, the diffusive distance would be 0.178 cm. Since this value is greater than the maximum height between the cone and the plate, this further supports the mapping of shear stress at the plate (endothelial) surface as of function of time as that defined by the input waveform under these temporal and geometric conditions.

Morphological and Migratory Response to Arterial Flow. Endothelial shape change *in vitro*, as well as established cell morphologies *in vivo*, prove to be faithful correlates of the nature of applied fluid shear stress [32,6,33,7]. To test the characteristic morphological response of an endothelial monolayer exposed to steady flow and to determine the corresponding mechanical adaptation to this new *in vitro* arterial flow condition, HUVEC were exposed to either 7.5 dyn/cm^2 of steady laminar shear stress (LSS) or arterial pulsatile flow (ART) with an equivalent time-averaged shear stress (7.5 dyn/cm^2) at a frequency of 1 Hz for 24 hours (Fig. 1b). After 24 hours, the cells exposed to LSS reoriented from a static monolayer of polygonal-shaped cells, with no preferred orientation, to a well characterized morphology in which the cells were elongated and aligned with the flow direction (Fig. 2a, top vs. middle panel). This elongation and alignment response seen for LSS also was observed for ECs exposed to ART (Fig. 2a, bottom panel). From time-lapse video microscopy, cell shape change, in terms of the aspect ratio (i.e., length of major axis/length of minor axis), was evaluated as a function of time. Within the first hour of flow onset, an immediate contractile response (i.e., cell rounding in shape, and a decrease in aspect ratio) was observed among individual cells within the monolayer, however, the integrity of the monolayer was maintained under both shear conditions. After 1 hour, the aspect ratio increased with the exposure time up to 18 hours of both LSS and ART, and reached maximum elongation in the direction of flow between 18 to 24 hours (24 hours: LSS, 2.03±0.07 vs. ART, 1.97±0.14, p>0.05; Fig. 2b). Temporal changes in the aspect ratio were similar for both flow conditions (p>0.05). These data suggest that cell shape change is dependent on the time-average shear stress, or net direction and magnitude of the flow vector, rather than temporal gradients in shear stress.

To gain further insight into how distinct flow patterns can influence cellular response, characteristics of cell migration were assessed under these two flow conditions. A baseline was first established by evaluating the migration patterns of confluent HUVEC under static (no flow) conditions for 24 hours. The experimental conditions for these static controls were identical to controls used for the shear counterparts, except instead of being stored in the incubator, the cells were enclosed in an incubator mounted on the microscope stage and maintained at 37°C and 5% CO$_2$ in humidified air. Figure 3a (left panel) shows the migratory pattern of multiple cells in a confluent monolayer under static conditions. HUVEC were observed to migrate in random patterns over 24 hours. In comparison, Figure 3a (middle and right panel) shows the representative migration patterns of individual cells exposed to LSS and ART conditions for 24 hours. Cells exposed to LSS had a smoother migratory pattern and translated greater distances compared to cells exposed ART. ART induced greater directional changes in its motion compared to LSS, although the total cumulative distances traveled by these cells were similar for each condition (data not shown). Observations made from time-lapse video microscopy showed that a majority of cells migrated in the direction of net flow and displayed continuous treading, or ruffling activity at the cell periphery, which lasted the duration of all three experimental conditions.

Although studies visualizing cell behavior under flow have focused on shape change or migratory pattern, none have characterized these spatial movements in the context of intrinsic migration
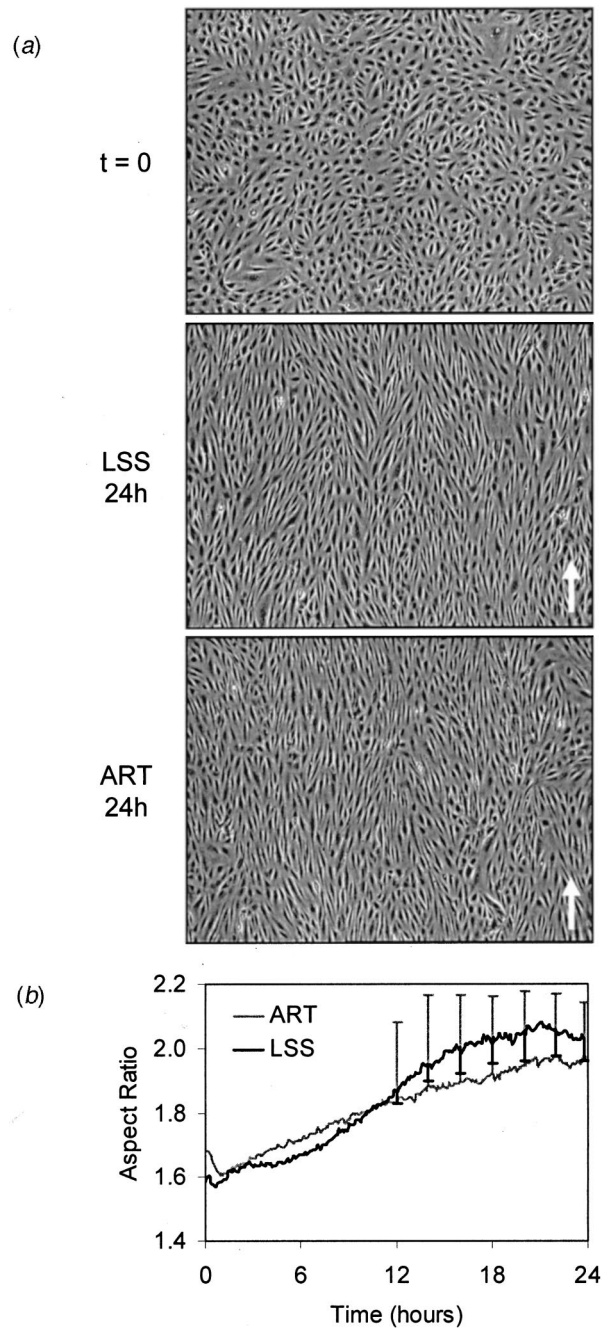

Fig. 2 Shear stress induced morphological changes in endothelial cells. (*a*) Images of HUVEC were acquired at the start of the experiment (t=0) and following 24 hours of LSS and ART. The arrow points in the direction of net flow. Images are representative of 3 independent experiments per condition. (*b*) Time-lapse video and image analysis techniques (see Methods) were used to evaluate changes in EC aspect ratio as a function of time (every 6 minutes) following 24 hours of exposure to LSS or ART. Curves were generated from the mean aspect ratio for each time point (LSS, n=3; ART, n=3). Standard error bars are plotted every 2 hours between 12 and 24 hours to illustrate non-significant differences among the LSS (black) and ART (gray) curves (p>0.05).

properties. Here we used the methods described by Dunn [27] to evaluate root mean square (RMS) cell speed and directional persistence from the mean square displacements (as described in the *Methods*). Directional persistence is defined as the average time
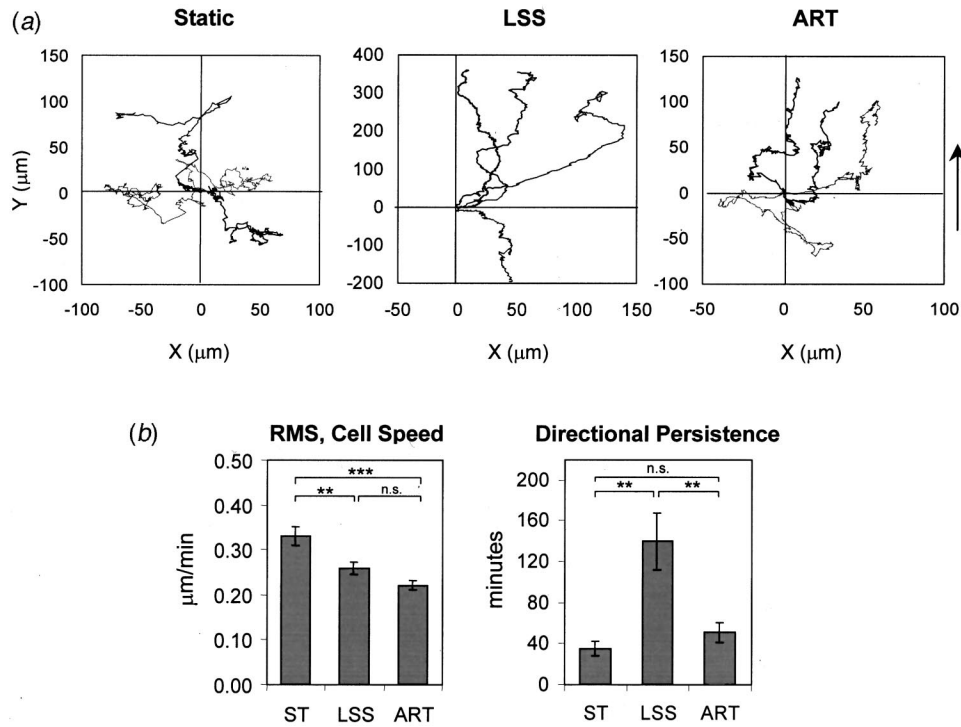
Fig. 3 Migration patterns and characteristics of HUVEC exposed to steady and arterial flow.
(*a*) Migratory patterns of four individual ECs (per plot) were tracked for 24 hours under static (no flow), LSS, and ART conditions. Traces of the cell's spatial movements are representative of the general migratory behaviors observed for that defined condition and were assessed from 3 independent experiments per condition. All distances were computed relative to a given cell's original centroid (at t=0), which is defined here as the origin. The arrow (right side) points in the direction of net forward flow for LSS and ART. (*b*) Intrinsic migratory characteristics, RMS cell speed (left) and directional persistence (right), were computed for 24 hours of static, LSS, and ART conditions from the equation describing the mean square displacements. Calculations were made from a total of 30 cells pooled from three independent experiments per condition. Bars represent the mean ±SE. **p<0.005, ***p<0.0001, n.s.=not significant.

between successive directional changes and can yield information regarding the generation of spatial movements. The static control was used again to acquire a baseline for this study. The basal RMS cell speed was found to be 0.33 ± 0.02 μm/min with P equal to 35.43 ± 7.07 minutes, validating the frequent directional changes seen in its migration pattern (Fig. 3*a*). The RMS cell speed of HUVEC was significantly reduced when exposed to either flow condition (LSS, 0.26 ± 0.01 and ART, 0.22 ± 0.01 μm/min, p<0.005 and p<0.0001, respectively; Fig. 3*b*). Cells exposed to ART migrated slightly slower (p>0.05) and with a dramatically reduced persistence time compared to cells under LSS (P: ART, 50.99 ± 9.16 vs. LSS, 140.08 ± 27.74 minutes, p<0.005; Fig. 3B). The directional persistence can be visually confirmed by the frequent jagged transitions in the migratory patterns of cells exposed ART in comparison to the longer persistence time and smoother trajectories under LSS.

Shear Stress Induced Remodeling of Cytoskeletal-Associated Proteins. Remodeling of the cytoskeleton, focal adhesions, and associated structural proteins in response to flow is a highly dynamic process that is dependent on the flow environment and plays an essential role in the temporal activation of mechanosensitive signaling pathways [2,14]. To further characterize the mechanical adaptation of the endothelium to arterial flow, structural-associated proteins, actin, plectin, and vinculin, were immunostained following 24 hours of LSS and ART. Confocal immunofluorescence microscopy was used to evaluate the apical stress fibers and plectin in a 1 μm thick region above the center of the nucleus, and vinculin in the basal compartment. LSS for 24 hours demonstrated a characteristic increase in apical stress fibers

that transverse the length of the cell, which were linearly oriented with its long axis, and were homogenously present in cells through the monolayer (Fig. 4*a*, center panel). In contrast, ECs exposed to ART exhibited a heterogeneous staining pattern of stress fibers within the morphologically oriented monolayer. A majority of these cells displayed fewer or no apical stress fibers, although many exhibited a thin cortical fiber structure (Fig. 4*a*, right panel). Vinculin, which localizes to focal adhesion sites on the basal surface of cells and aides in the linkage of stress fibers to integrin structures [34], was reported to localize into linear plaques in the upstream side of ECs exposed to LSS [35,8] and cell periphery [36]. A detergent extracted protocol was used prior to fixation to remove diffuse cytosolic staining of vinculin in order to clearly visualize detergent-resistant vinculin complexes. Here vinculin orients into strong linear adhesion plaques localized throughout the cell (Fig. 4*b*, center panel) and co-localized with the ends of stress fibers after 24 hours of LSS (data not shown). For arterial flow, however, these vinculin-stained plaques were more punctate and diffuse within cells, and the linear plaques were smaller, sparse and heterogeneous throughout the monolayer (Fig. 4*b*, right panel). Similar staining patterns of vinculin complexes were also observed when cells were fixed prior to being permeablized (data not shown). While differences in staining pattern were observed for the above proteins, staining of the abundant cytoskeletal protein linker, plectin, showed no qualitative difference in staining pattern or distribution (Fig. 4a). The plectin structure remodeled from a random, non-oriented pattern under static conditions to a more linear pattern along the cell's major
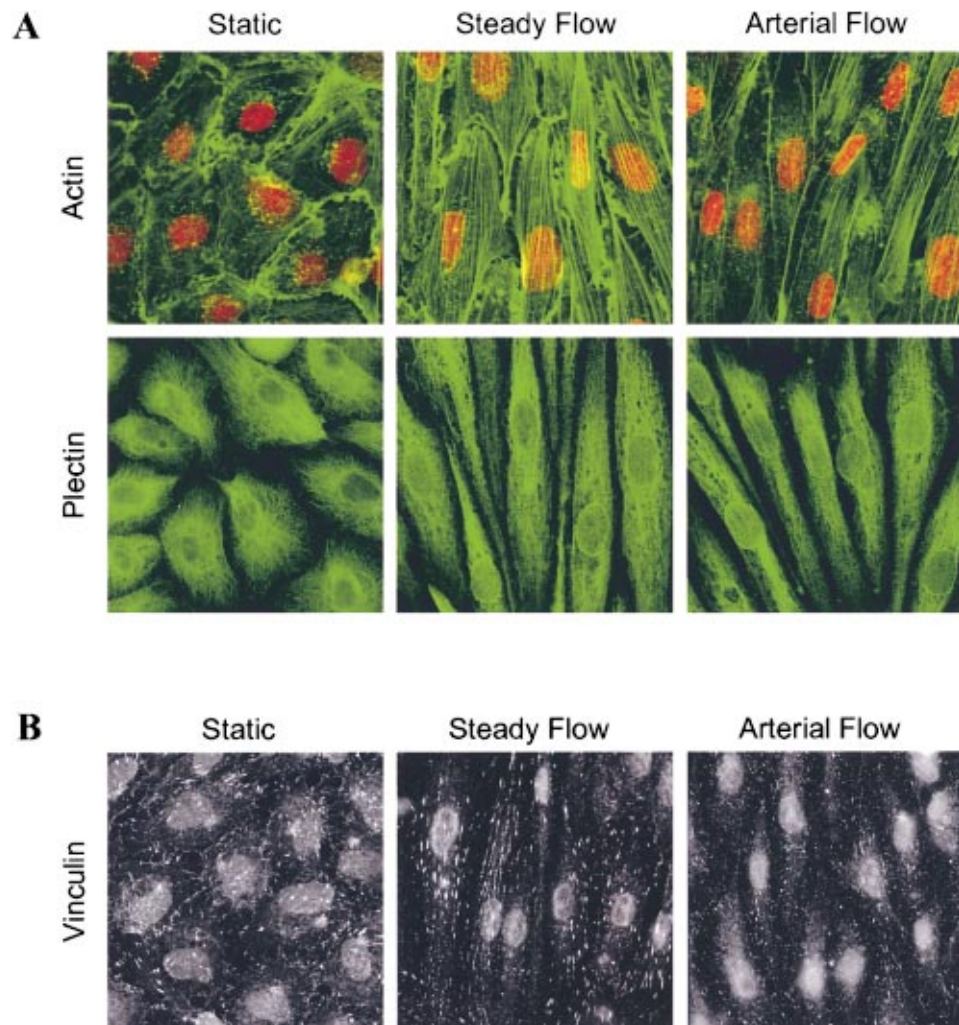
Fig. 4 Remodeling of cytoskeletal-associated structures following 24 hours of arterial and steady shear stress. Confocal immunofluorescence micrographs show the distribution of (a) actin and plectin in the apical (supranuclear) compartment, and (b) vinculin, in basal compartment, in HUVEC after exposure to static (left), LSS (middle), and ART (right) for 24 hours. Actin stress fibers (top) are stained green and the nuclei counterstained with SYTOX (red). Images are representative of four independent experiments per condition.

axis following exposure to LSS and ART for 24 hours. Other proteins such as vimentin and microtubules also showed no difference in staining pattern (data not shown).

eNOS is Modulated by Distinct Shear Stress Patterns. Endothelial cell production of nitric oxide has been shown to be highly responsive to the flow environment *in vitro* and *in vivo*, reflecting immediate changes in enzymatic activity and short and long-term increases in endothelial nitric oxide synthase (eNOS) expression at both the mRNA and protein levels [37–41]. To examine the regulation of eNOS expression by ART *in vitro*, we measured changes in protein and gene expression after 6 or 24 hours of ART or LSS relative to static controls. Figure 5a shows no change in the amount of protein following 6 hours of LSS or ART (LSS 0.83 ± 0.40 vs. ART 1.41 ± 0.09 arbitrary units, $p=0.23$). In contrast, a significant increase in eNOS protein was observed for LSS after 24 hours, but not for ART (LSS 4.03 ± 0.60 vs. ART 1.35 ± 0.46, $p<0.05$). Evaluation of gene expression revealed a different trend. An increase in eNOS gene expression was observed following 6 hours of steady flow (1.73 ± 0.028) that was sustained through 24 hours (2.10 ± 0.28; Fig. 5b). Endothelial cells exposed to ART, however, had a modest increase in expression at 6 hrs, which increased to values similar to LSS after 24 hours

relative to static control cells (ART 6 h, 1.14 ± 0.13, 24 h, 1.81 ± 0.21). For this time course, these data demonstrate that arterial flow does not alter the amount of eNOS protein up to 24 hrs of flow, though gene expression was upregulated by 24 hours. Earlier activation of the gene was more sensitive to steady flow rather than dynamic time-varying pulsatile flow at this frequency.

Discussion. For the past twenty years, research has aimed at modeling various flow conditions on endothelium *in vitro* in order to understand how biomechanical forces (i.e., shear stress) affect cellular responses. Although these studies have identified many flow responsive pathways, most have focused on modeling the flow environment with steady, sinusoidal, or turbulent flow conditions [2], which do not possess the complex time-varying features of *in vivo* blood flow [1]. In the present study, we described the development of a novel *in vitro* model to simulate the shear stress component of human blood flow waveforms on cultured endothelial cells. An arterial-like shear stress waveform modified from a previously characterized blood velocity measurements from the abdominal aorta of normal human subject [22] was successfully modeled in our DFS and tested by evaluating the biological response of ECs to this new type of flow profile.
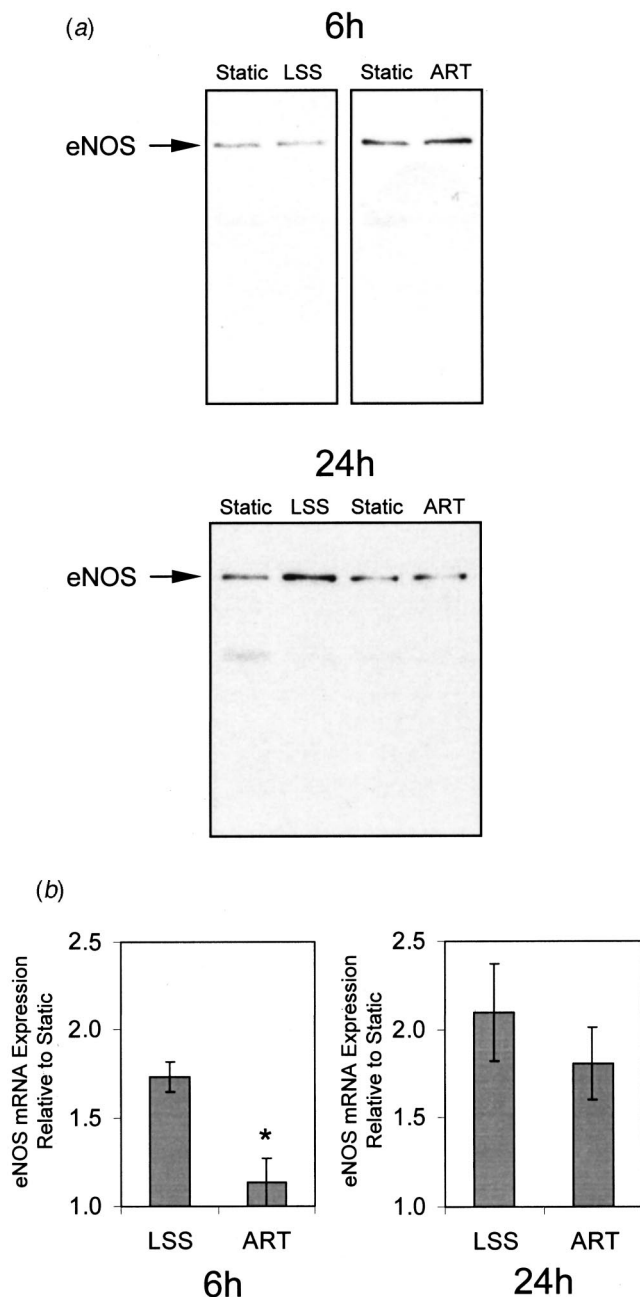
Fig. 5 Shear stress induced regulation of eNOS protein and mRNA expression in HUVEC. (*a*) Western blot for eNOS protein following 6 and 24 hours of LSS and ART flow. Static samples represent no flow time-matched controls for each experimental condition. Samples were equally loaded with $50\mu g$ of protein, and blots are representative of 3 independent experiments per condition (Densitometry analysis normalized to static experiment: LSS 6h 0.83 ± 0.40 vs. ART6h 1.41 ± 0.09 arbitrary units, $p=0.23$; LSS 24h 4.03 ± 0.60 vs. ART 24h 1.35 ± 0.46 arbitrary units, $p<0.05$). (*b*) Relative mRNA levels of eNOS following 6 and 24 hours of LSS and ART were measured by real-time PCR (Taqman). Measurements were made in duplicate from three independent experiments. Results were normalized using $\beta2$ microglobulin, a gene not regulated by these stimuli. Bars represent mean $\pm$SE (LSS: 6h, n=3, 24h, n=3; ART: 6h, n=3, 24h, n=4). *p<0.05.

Endothelial morphology and orientation in arteries *in vivo* correlates with the local hemodynamic environment [32,33]. Similar results have also been observed with steady and pulsatile shear stress patterns *in vitro* [6,42]. Here we show ECs exposed to either arterial flow or the equivalent time-average steady shear stress cause cells to change shape in a similar manner over 24 hours, from a polygonal morphology to one that is aligned with the direction of flow (Fig. 2b), similar to ECs in straight non-bifurcating arterial segment [32]. This result is in agreement with several studies indicating that cell shape change, up to 24 hours, is dependent on the magnitude (i.e., time-average shear stress) rather than temporal gradients in shear stress [7,9]. However, in some cases of non-reversing and reversing sinusoidal flows, the time course of realignment is slower compared to its steady, time-averaged counterpart, although cell shape by 24 hours is comparable [7]. This general finding does not hold for turbulent flow where the shape of the cells remains relatively polygonal in comparison to an equivalent LSS stimulus [11], thus indicating the importance of the direction and magnitude of the flow vector. The conclusion that cell morphology at 24 hours is dependent on the time-average shear stress was based on pulsatile flow studies conducted at frequencies of 1 Hz. To accurately develop this concept into a working hypothesis, work is currently underway to evaluate the effect of frequency on cell shape response.

Evaluating endothelial migration patterns and characteristics under static and distinct fluid shear stress conditions has revealed interesting results that may provide insight into the activation of mechanisms involved in cell motility and mechanotransduction. Here we show that ECs under LSS (7.5 dyn/cm^2) and ART experienced a $\sim20\%$ and $\sim30\%$ decrease in RMS cell speed, respectively, relative to a static confluent monolayer over the same 24 hour time period. Although this observation has not been previously reported, a dramatic decrease in spatial fluctuation around the mean trajectories of bovine ECs had been observed following the onset of steady flow causing a reduction in random movement [43]. The reduction in RMS cell speed, in general, suggests that shear stress is activating mechanisms that lead to the resistance in motion. Two such mechanisms could include an increase in the engagement of integrins or activation of proteins decreasing actin-based motility. Focal adhesions (FA) in ECs continuously remodel under static conditions, which most likely contributes to their random migratory patterns seen graphically in Figure 2a, but the rate of FA remodeling does not significantly change following the exposure to flow up to 24 hours [44]. Even though integrin ligation is an early mechanically induced event [5], the data reported by Davies et al. [44] suggests there is no net change in the number of adhesions being made. The observed decrease in speed may therefore reflect an increase in vinculin association with FA rather than an increase in integrin adhesion. An increase in vinculin expression in 3T3 cells increases FA and stress fiber formation and reduces cell motility [45], which is reversible with an antisense gene to decrease vinculin expression [46]. Additional evidence from vinculin deficient cells demonstrates a decrease in mechanical stiffness that increases when vinculin is expressed into these cells [47]. When vinculin localizes to FA, it recruits adaptor proteins that facilitates its linkage from integrins to stress fibers creating a mechanical connection to the extracellular matrix [34]. These findings support the hypothesis that an increase in association of vinculin to FA increases the resistance to motion by providing an increase in mechanical strength between the extracelluar matrix and cytoskeleton. Actin dynamics at the leading edge of a cell is another mechanism essential for cell migration. A recent report using a wound assay of BAECs found that actin filament turnover rate positively correlates with RMS cell speed in ECs [48]. This result suggests that distinct shear stress patterns can modulate the activity of proteins critical in actin-based motility and may explain differences in RMS cell speed reported here as well as differences observed in velocity measurements in EC exposed to defined spatial gradients of shear stress, elsewhere [49].

Another interesting observation is cells exposed to arterial flow experienced a 15% reduction in cell speed compared to LSS and a 64% reduction in persistence time. Although an obvious math-

ematical relationship links these two variables, future studies are warranted to investigate the cellular mechanisms responsible for dramatic differences seen between them. In this study, S and P were computed over 24 hours, however, a more detailed analysis is underway to assess these intrinsic variables at a finer resolution (e.g., every 3 hr) to provide greater temporal detail for short and long term cell migration and determine how this may influence mechanotransduction and correlate with changes in cell phenotype. This study demonstrates that the flow environment, per se, influences intrinsic migratory properties of HUVEC.

In vivo studies have demonstrated a correlation between cell shape, actin stress fibers, and the hemodynamic environment [50,51] as well as demonstrated a direct effect of altered flow on cell morphology and stress fiber distribution [52]. Similar findings have been reported for ECs *in vitro* exposed to LSS in which there is an increase in the number of parallel oriented stress fibers that span the length of the cell's major axis [53,54] and the apical region of the nucleus, as shown in this study, and previously [14]. Here we show ECs exposed to ART exhibit a significant reduction in the number of centrally oriented stress fibers in the apical region of cells following 24 hours of flow with an overall heterogeneous distribution of stress fibers within the monolayer relative to LSS. Similar heterogeneity has been observed *in vivo* [55,52], however this pattern is unlike any previously reported *in vitro*. Cells exposed to pulsatile flows, such as, sinusoidal flows exhibit stress fiber staining similar to LSS, but form thicker fibers, whereas ECs exposed to oscillatory flows either have no [7], or random-oriented, central fibers [9]. Together, these data indicate that shear stress can modulated actin stress fiber structure and strengthens the argument that the exact nature of the shear stress waveform is an important predictor of stress fiber formation and distribution, which may have implications to its function in shear-stimulated ECs.

eNOS plays a critical role in maintaining the contractile, remodeling and homeostatic environment of arteries [56,57] and has been shown to be highly responsive to flow *in vitro*. We evaluated the regulation of eNOS mRNA and protein expression by arterial shear stress *in vitro* and compared it to the well studied LSS stimulus. In this study, a significant increase in eNOS mRNA was detected after 6 hours of LSS and sustained at the same level up to 24 hours. However, a significant increase in protein expression was only observed at 24 hours, similar to a previous report [38]. Arterial flow showed a modest increase in eNOS mRNA at 6 hours and greater increase at 24 hours, though protein expression remained unchanged at both time points relative to static controls. These data suggest that the regulation of eNOS mRNA in HUVEC is more sensitive to steady rather than arterial pulsatile shear stress at earlier times (i.e., 6 hours) and possibly dependent on the equivalent time-average shear stress or a continual exposure to flow at longer time points (i.e., 24 hours). In support of these data, recent work in bovine aortic ECs demonstrated a greater increase in eNOS mRNA at 6 hours of LSS (20 dyn/cm^2) compared to an oscillatory waveform (sinusoidal, $\pm 20 \text{ dyn/cm}^2$, 1 Hz), with increasing trends for each condition up to 9 hours [58]. The transient increase in mRNA levels with pulsatile flow is a trend not observed by turbulent flow in which there is no change in eNOS mRNA at 6 hours [12] and 24 hours [13]. This demonstrates that the regulation of eNOS mRNA is dependent on the type of shear stress waveform, perhaps reflecting its acceleration/deceleration components. As for eNOS protein levels, a sustained increase in mRNA appears to be necessary for the increase in protein as reported for LSS (20 dyn/cm^2) at 4 and 8-hours [59] and LSS (15 dyn/cm^2) [38,60] and forward oscillatory flow (3 to 9 dyn/cm^2, 1 Hz, with pulse pressure) [61] at 24 hours.

Recent investigations have focused on modulating the temporal component of shear stress functions (e.g., trapezoidal or sinusoidal function) as a means of examining the unsteady component of shear stress patterns *in vivo* and identifying rate sensitive signal pathways and mechanotransduction mechanisms in ECs *in vitro*.

Data from this work has revealed differential responses in signaling molecules [42,62] and the expression of proteins and genes that depend on the temporal gradient of shear stress [63–65]. These results may provide insight into similar features, such as the shear stress rate, that associate with more complex waveforms of an arterial flow function. We are actively using this model to investigate mechanisms sensitive to the temporal characteristics of unsteady flow in order to understand the rate sensitivity of the endothelium.

Conclusion

In this study, we have presented the groundwork for a new *in vitro* model used to simulate the shear stress component of *in vivo* blood flow on ECs in culture. The DFS does not, however, incorporate the additional stress components, hydrostatic pressure and hoop stress, encountered by the endothelium *in vivo*. A more comprehensive model, which imposes all three stress components, may facilitate our understanding of the complex regulation of these forces on EC response in an intact vessel. In order to understand the relative contribution of the complex shear stress component of arterial flows on EC response, we have developed, as a first step, this arterial shear stress model to provide a more exact relationship between a well-defined biomechanical force and a measurable biological response. As a starting point, we set out to fully characterize this new type of arterial-like waveform on the biological response of HUVEC. Here we show that the exposure of ECs to ART caused changes in intrinsic cell migratory properties, distribution of actin stress fibers and vinculin cytoskeletal structures, and regulation of eNOS mRNA and protein expression, but not cell shape change or RMS cell speed compared to an equivalent LSS. This study represents the initial report characterizing the biological responses of ECs to an arterial-like shear stress flow environment. Future studies are aimed at evaluating the effect of arterial frequency and amplitude on EC response in order to understand how ECs sense shear stress and decode various components (e.g., amplitude, frequency, flow reversal) of an arterial waveform. These data further support observations that the endothelial cells can not only sense, but also discriminate among distinct shear stress stimuli [12–14] and demonstrate the utility of an arterial flow model to provide greater insight into the coordination of mechanisms involved in mechano-sensing and modulation of endothelial phenotype.

Nomenclature

α = cone angle
μ = dynamic viscosity
τ = shear stress
ν = kinematic viscosity
ω = angular velocity
ω_f = frequency
$\langle D^2 \rangle$ = mean squared displacement
P = directional persistence time
S = root mean square (rms) cell speed
T = time interval
ART = arterial pulsatile flow
cP = centipoises
DFS = dynamic flow system
EC = endothelial cell
eNOS = endothelial cell nitric oxide synthase

HUVEC = human umbilical vein endothelial cells
LSS = laminar shear stress

References

[1] Nichols, W. W., O'Rourke, M. F., Hartley, C., and McDonald, D. A., 1998, *McDonald's Blood Flow In Arteries: Theoretical, Experimental, and Clinical Principles*, Oxford Press, New York.

[2] Davies, P. F., 1995, "Flow-mediated Endothelial Mechanotransduction," Physiol. Rev., **75**(3), pp. 519–560.

[3] Traub, O., and Berk, B. C., 1998, "Laminar Shear Stress: Mechanisms by Which Endothelial Cells Transduce an Atheroprotective Force," Arterioscler., Thromb., Vasc. Biol., **18**(5), pp. 677–685.

[4] Haidekker, M. A., L'Heureux, N., and Frangos, J. A., 2000, "Fluid Shear Stress Increases Membrane Fluidity in Endothelial Cells: A Study with DCVJ Fluorescence," Am J Physiol Heart Circ Physiol, **278**(4), pp. H1401–H1406.

[5] Jalali, S., del Pozo, M. A., Chen, K., Miao, H., Li, Y., Schwartz, M. A., Shyy, J. Y., and Chien, S., 2001, "Integrin-mediated Mechanotransduction Requires its Dynamic Interaction With Specific Extracellular Matrix Ligands," Proc. Natl. Acad. Sci. U.S.A., **98**(3), pp. 1042–1046.

[6] Dewey, C. F., Jr., Bussolari, S. R., Gimbrone, M. A., Jr., and Davies, P. F., 1981, "The Dynamic Response of Vascular Endothelial Cells to Fluid Shear Stress," J. Biomech. Eng., **103**(3), pp. 177–185.

[7] Helmlinger, G., Geiger, R. V., Schreck, S., and Nerem, R. M., 1991, "Effects of Pulsatile Flow on Cultured Vascular Endothelial Cell Morphology," J. Biomech. Eng., **113**(2), pp. 123–131.

[8] Girard, P. R., and Nerem, R. M., 1995, "Shear Stress Modulates Endothelial Cell Morphology and f-actin Organization Through the Regulation of Focal Adhesion-associated Proteins," J. Cell Physiol., **163**, pp. 179–193.

[9] Thoumine, O., Nerem, R. M., and Girard, P. R., 1995, "Oscillatory Shear Stress and Hydrostatic Pressure Modulate Cell-matrix Attachment Proteins in Cultured Endothelial Cells," In Vitro Cellular & Developmental Biology, Animal, **31**(1), pp. 45–54.

[10] DePaola, N., Gimbrone, M. A. Jr., Davies, P. F., and Dewey, C. F., Jr., 1992, "Vascular Endothelium Responds to Fluid Shear Stress Gradients [published erratum appears in Arterioscler Thromb 1993 Mar; **13**(3) p. 465]," Arterioscler. Thromb., **12**(11), pp. 1254–1257.

[11] Davies, P. F., Remuzzi, A., Gordon, E. J., Dewey, C. F., Jr., and Gimbrone, M. A., Jr., 1986, "Turbulent Fluid Shear Stress Induces Vascular Endothelial Cell Turnover In Vitro," Proc. Natl. Acad. Sci. U.S.A., **83**(7), pp. 2114–2117.

[12] Noris, M., Morigi, M., Donadelli, R., Aiello, S., Foppolo, M., Todeschini, M., Orisio, S., Remuzzi, G., and Remuzzi, A., 1995, "Nitric Oxide Synthesis by Cultured Endothelial Cells is Modulated by Flow Conditions," Circ. Res., **76**(4), pp. 536–543.

[13] Topper, J., Cai, J., Falb, D., and Gimbrone, M. A., Jr., 1996, "Identification of Vascular Endothelial Genes Differentially Responsive to Fluid Mechanical Stimuli: Cyclooxygenase-2, Manganese Superoxide Dismutase, and Endothelial Cell Nitric Oxide Synthase are Selectively Up-regulated by Steady Laminar Shear Stress," Proc. Natl. Acad. Sci. U.S.A., **98**, pp. 10417–10422.

[14] Garcia-Cardena, G., Comander, J., Anderson, K. R., Blackman, B. R., and Gimbrone, M. A., Jr., 2001, "Biomechanical Activation of Vascular Endothelium as a Determinant of its Functional Phenotype," Proc. Natl. Acad. Sci. U.S.A., **98**(8), pp. 4478–4485.

[15] Gimbrone, M. A. J., Topper, J. N., Nagel, T., Anderson, K. R., and Garcia-Cardena, G., 2000, "Endothelial Dysfunction, Hemodynamic Forces, and Atherogenesis," Ann NY Acad Sci, **902**, pp. 230–239.

[16] Moore, J. E., Jr., Burki, E., Suciu, A., Zhao, S., Burnier, M., Brunner, H. R., and Meister, J. J., 1994, "A Device for Subjecting Vascular Endothelial Cells to Both Fluid Shear Stress and Circumferential Cyclic Stretch," Ann. Biomed. Eng., **22**(4), pp. 416–422.

[17] Peng, X., Recchia, F. A., Byrne, B. J., Wittstein, I. S., Ziegelstein, R. C., and Kass, D. A., 2000, "In Vitro System to Study Realistic Pulsatile Flow and Stretch Signaling in Cultured Vascular Cells," Am J Physiol Cell Physiol, **279**, pp. C797–C805.

[18] Qiu, Y., and Tarbell, J. M., 2000, "Interaction Between Wall Shear Stress and Circumferential Strain Affects Endothelial Cell Biochemical Production," J. Vasc. Res., **37**(3), pp. 147–157.

[19] Langille, B. L., 1984, "Integrity of Arterial Endothelium Following Acute Exposure to High Shear Stress," Biorheology, **21**, pp. 333–346.

[20] Schnittler, H. J., Franke, R. P., Akbay, U., Mrowietz, C., and Drenckhahn, D., 1993, "Improved In Vitro Rheological System for Studying the Effect of Fluid Shear Stress on Cultured Cells," Am. J. Physiol., **265**(1 Pt 1), pp. C289–298.

[21] Blackman, B. R., Barbee, K. A., and Thibault, L. E., 2000, "In Vitro Cell Shearing Device to Investigate the Dynamic Response of Cells in a Controlled Hydrodynamic Environment," Ann. Biomed. Eng., **28**(4), pp. 363–372.

[22] Maier, S. E., Meier, D., Boesiger, P., Moser, U. T., and Vieli, A., 1989, "Human Abdominal Aorta: Comparative Measurements of Blood Flow with MR Imaging and Multigated Doppler US.," Radiology, **171**(2), pp. 487–492.

[23] Oshinski, J. N., Ku, D. N., Mukundan, S. J., Loth, F., and Pettigrew, R. I., 1995, "Determination of Wall Shear Stress in the Aorta With the Use of MR Phase Velocity Mapping," J. Magn. Reson Imaging, **5**(6), pp. 640–647.

[24] Oyre, S., Pedersen, E. M., Ringgaard, S., Boesiger, P., and Paaske, W. P., 1997, "In Vivo Wall Shear Stress Measured by Magnetic Resonance Velocity Mapping in the Normal Human Abdominal Aorta," Eur. J. Vasc. Endovasc Surg., **13**(3), pp. 263–271.

[25] Ling, S. C., Atabek, H. B., Letzing, W. G., and Patel, D. J., 1973, "Nonlinear Analysis of Aortic Flow in Living Dogs," Circ. Res., **33**(2), pp. 198–212.

[26] Ling, S. C., and Atabek, H. B., 1972, "A Nonlinear Analysis of Pulsatile Flow in Arteries," J. Fluid Mech., **55**, pp. 493–511.

[27] Dunn, G. A., 1983, Characterizing a Kinesis Response: Time Averaged Measures of Cell Speed and Directional Persistence. *Leukocyte Locomotion and Chemotaxis*, H. O. Keller and G. O. Till. Basel, Birkhauser: pp. 14–33.

[28] Ku, D. N., Giddens, D. P., Zarins, C. K., and Glagov, S., 1985, "Pulsatile Flow and Atherosclerosis in the Human Carotid Bifurcation. Positive Correlation Between Plaque Location and Low Oscillating Shear Stress," Arteriosclerosis (Dallas), **5**(3), pp. 293–302.

[29] Moore, J. E. J., Xu, C., Glagov, S., Zarins, C. K., and Ku, D. N., 1994, "Fluid Wall Shear Stress Measurements in a Model of the Human Abdominal Aorta: Oscillatory Behavior and Relationship to Atherosclerosis," Arteriosclerosis (Dallas), **110**(2), pp. 225–240.

[30] Fewell, M. E., and Hellums, J. D., 1977, "The Secondary Flow of Newtonian Fluids in a Cone-and-Plate Viscometers," Trans. Soc. Rheol., **21**, pp. 535–565.

[31] Sdougos, H. P., Bussolari, S. R., and Dewey, C. F., 1984, "Secondary Flow and Turbulence in a Cone-and-Plate Device," J. Fluid Mech., **138**, pp. 379–404.

[32] Silkworth, J. B., and Stephbens, W. E., 1975, "The Shape of Endothelial Cells in en face Preparations of Rabbit Blood Vessels," Angiology, **26**, pp. 474–487.

[33] Langille, B. L., and Adamson, S. L., 1981, "Relationship Between Blood Flow Direction and Endothelial Orientation at Arterial Branch Sites in Rabbits and Mice," Circ. Res., **48**, pp. 481–488.

[34] Burridge, K., Molony, L., and Kelly, T., 1987, "Adhesion Plaques: Sites of Transmembrane Interaction Between the Extracellular Matrix and the Actin Cytoskeleton," J. Cell Sci. Suppl., **8**, pp. 211–229.

[35] Girard, P. R., and Nerem, R. M., 1993, "Endothelial Cell Signaling and Cytoskeletal Changes in Response to Shear Stress," Front Med. Biol. Eng., **5**(1), pp. 31–36.

[36] Galbraith, C. G., Skalak, R., and Chien, S., 1998, "Shear Stress Induces Spatial Reorganization of the Endothelial Cell Cytoskeleton," Cell Motil. Cytoskeleton, **40**(4), pp. 317–330.

[37] Rubanyi, G. M., Romero, J. C., and Vanhoutte, P. M., 1986, "Flow-induced Release of Endothelium-Derived Relaxing Factor," Am. J. Physiol., **250**, pp. H1145–H1149.

[38] Nishida, K., Harrison, P. G., Navas, J. P., Fisher, A. A., Dockery, S. P., Uematsu, M., Nerem, R. M., Alexander, R. W., and Murphy, T. J., 1992, "Molecular Cloning and Characterization of the Constitutive Bovine Aortic Endothelial Cell Nitric Oxide Synthase," J. Clin. Invest., **90**(5), pp. 2092–2096.

[39] Kuchan, M. J., and Frangos, J. A., 1994, "Role of Calcium and Calmodulin in Flow-Induced Nitric Oxide Production in Endothelial cells," Am. J. Physiol., **266**(3 Pt 1), pp. C628–636.

[40] Sessa, W. C., Pritchard, K., Seyedi, N., Wang, J., and Hintze, T., 1994, "Chronic Exercise in Dogs Increases Coronary Vascular Nitric Oxide Production and Endothelial Cell Nitric Oxide Synthase Gene Expression," Circ. Res., **74**(2), pp. 349–353.

[41] Davis, M. E., Cai, H., Drummond, G. R., and Harrison, D. G., 2001, "Shear Stress Regulates Endothelial Nitric Oxide Synthase Expression Through C-src by Divergent Signaling Pathways," Circ. Res., **89**, pp. 1073–1080.

[42] Helmlinger, G., Berk, B. C., and Nerem, R. M., 1995, "Calcium Responses of Endothelial Cell Monolayers Subjected to Pulsatile and Steady Laminar Flow Differ," Am. J. Physiol., **269**(2 Pt 1), pp. C367–375.

[43] Dieterich, P., Odenthal-Schnittler, M., Mrowietz, C., Kramer, M., Sasse, L., Oberleithner, H., and Schnittler, H. J., 2000, "Quantitative Morphodynamics of Endothelial Cells Within Confluent Cultures in Response to Fluid Shear Stress," Biophys. J., **79**, pp. 1285–1297.

[44] Davies, P. F., Robotewskyj, A., and Griem, M. L., 1994, "Quantitative Studies of Endothelial Cell Adhesion. Directional Remodeling of Focal Adhesion Sites in Response to Flow Forces," J. Clin. Invest., **93**(5), pp. 2031–2038.

[45] Rodriquez Fernandez, J. L., Geiger, B., Salomon, D., and Ben-Ze'ev, A., 1992, "Overexpression of Vinculin Suppresses Cell Moltility in BALB/c 3T3 Cells," Cell Motil. Cytoskeleton, **22**, pp. 127–134.

[46] Rodriquez Fernandez, J. L., Geiger, B., Salomon, D., Sabanay, I., Zoller, M., and Ben-Ze'ev, A., 1992, "Suppression of Tumorigenicity in Transformed Cells After Transfection With Vinculin cDNA," J. Cell Biol., **119**(2), pp. 427–438.

[47] Ezzell, R. M., Goldmann, W. H., Wang, N., Parasharama, N., and Ingber, D. E., 1997, "Vinculin Promotes Cell Spreading by Mechanically Coupling Integrins to the Cytoskeleton," Exp. Cell Res., **231**, pp. 14–26.

[48] McGrath, J. L., Osborn, E. A., Tardy, Y. S., Dewey, C. F., Jr., and Hartwig, J. H., 2000, "Regulation of the Actin Cycle In Vivo by Actin Filament Severing," Proc. Natl. Acad. Sci. USA, **97**(12), pp. 6532–6537.

[49] Tardy, Y., Resnick, N., Nagel, T., Gimbrone, Jr., M. A., and Dewey, Jr., C. F., 1997, "Shear Stress Gradients Remodel Endothelial Monolayers In Vitro Via a Cell Proliferation-Migration-Loss Cycle," Arterioscler., Thromb., Vasc. Biol., **17**(11), pp. 3102–3106.

[50] White, G. E., and Gimbrone, M. A., Jr., 1983, "Factors Influencing the Expression of Stress Fibers In Vascular Endothelial Cells In Situ," J. Cell Biol., **97**, pp. 416–424.

[51] Wong, A. J., and Herman, I. M., 1983, "Actin Filament Stress Fibers In Vascular Endothelial Cells In Vivo," Science, **219**, pp. 867–869.

[52] Kim, D. W., Gotlieb, A. I., and Langille, B. L., 1989, "In Vivo Modulation of Endothelial F-actin Microfilaments by Experimental Alterations in Shear Stress," Arteriosclerosis (Dallas), **9**(4), pp. 439–445.

[53] Franke, R. P., Grafe, M., Schnittler, H., Seiffge, D., and Mittermayer, C., 1984,

"Induction of Human Vascular Endothelial Stress Fibers by Fluid Shear Stress," Nature, **307**, pp. 648–649.

[54] Wechezak, A. R., Viggers, R. F., and Sauvage, L. R., 1985, "Fibronectin and *f*-actin Redistribution in Cultured Endothelial Cells Exposed to Shear Stress," Lab Invest, **53**(6), pp. 639–647.

[55] White, G. E., and Fujiwara, K., 1986, "Expression and Intracellular Distribution of Stress Fibers in Aortic Endothelium," J. Cell Biol., **103**(1), pp. 63–70.

[56] Rudic, R. D., Shesely, E. G., Maeda, N., Smithies, O., Segal, S. S., and Sessa, W. C., 1998, "Direct Evidence for the Importance of Endothelium-derived Nitric Oxide In Vascular Remodeling," J. Clin. Invest., **101**(4), pp. 731–736.

[57] Papapetropoulos, A., Rudic, R. D., and Sessa, W. C., 1999, "Molecular Control of Nitric Oxide Synthases in the Cardiovascular System," Cardiovasc. Res., **43**(3), pp. 509–520.

[58] Malek, A. M., Izumo, S., and Alper, S. L., 1999, "Modulation by Pathophysiological Stimuli of the Shear Stress-induced Up-regulation of Endothelial Nitric Oxide Synthase Expression in Endothelial Cells," Neurosurgery, **45**(2), pp. 334–344.

[59] Wedgewood, S., Bekker, J. M., and Black, S. M., 2001, "Shear Stress Regulation of Endothelial NOS in Fetal Pulmonary Arterial Endothelial Cells Involves PKC," Am J Physiol Lung Cell Mol Physiol, **281**, pp. L490–L498.

[60] Uematsu, M., Ohara, Y., Navas, J. P., Nishida, K., Murphy, T. J., Alexander, R. W., Nerem, R. M., and Harrison, D. G., 1995, "Regulation of Endothelial Cell Nitric Oxide Synthase mRNA Expression by Shear Stress," Am. J. Physiol., **269**, pp. C1371–C1378.

[61] Ziegler, T., Bouzourene, K., Harrison, V. J., Brunner, H. R., and Hayoz, D., 1998, "Influence of Oscillatory and Unidirectional Flow Environments on the Expression of Endothelin and Nitric Oxide Synthase in Cultured Endothelial Cells," Arterioscler., Thromb., Vasc. Biol., **18**(5), pp. 686–692.

[62] Blackman, B. R., Thibault, L. E., and Barbee, K. A., 2000, "Selective Modulation of Endothelial Cell $[Ca^{2+}]_i$ Response to Flow by the Onset Rate of Shear Stress," J. Biomech. Eng., **122**(3), pp. 274–282.

[63] Bao, X., Lu, C., and Frangos, J., 1999, "Temporal Gradient in Shear but not Steady Shear Stress Induces PDGF-A and MCP-1 Expression in Endothelial Cells; Role of NO, NFκB, and egr-1," Arterioscler., Thromb., Vasc. Biol., **19**, pp. 996–1003.

[64] Bao, X., Clark, C. B., and Frangos, J. A., 2000, "Temporal Gradient in Shear-induced Signaling Pathway: Involvement of MAP Kinase, c-fos, and Connexin-43," Am J Physiol Heart Circ Physiol, **278**, pp. H1598–H1605.

[65] Bao, X., Lu, C., and Frangos, J. A., 2001, "Mechanism of Temporal Gradients in Shear-induced ERK1/2 Activation and Proliferation in Endothelial Cells," Am J Physiol Heart Circ Physiol, **281**(1), pp. H22–29.